Optica Applicata, Vol. LII, No. 2, 2022
DOI: 10.37190/oa220201

Optical design of a short-wave infrared coded aperture snapshot spectral imager based on Offner–Wynne imaging spectrometer

Chong Song[1, 2*], Liang Zhou[1], Zhaohui Liu[1], Kai Jiang[1], Kai Liu[1]

[1]Xi'an Institute of Optics and Precision Mechanics of Chinese Academy of Sciences, Xi'an 710000, China

[2]University of Chinese Academy of Sciences, Beijing 100049, China

[*]Corresponding author.: songchong124@163.com

A calculation model to obtain the optimal combination of Offner–Wynne imaging spectrometer parameters to balance the RMS spot radius of the chief ray over the entire field is established. On the basis of the calculation model, an Offner–Wynne imaging spectrometer is designed, and then it is applied in a short-wave infrared coded aperture snapshot spectral imager (CASSI). The optical system of the short-wave infrared CASSI is designed by a combination method of independent design and integrated optimization. The spectral smile and spectral keystone of the optical system which operates in the 900–1700 nm band are respectively less than half a pixel. The focal length of the optical system is 1200 mm, the total optical system length is 775 mm, and its average spectral resolution is 16 nm. The optical system offers the advantages of excellent imaging quality, compact optical structure, high optical transmittance, reduced spectral smile and spectral keystone.

Keywords: Offner–Wynne imaging spectrometer, CASSI, short-wave infrared, optical design.

1. Introduction

Imaging spectrometers have played an important role in various areas such as remote sensing, medicine, environment, astrophysics, and military detection [1–4]. Traditional spectral imaging often includes data scanning, either the wavelength or spatial axis, which is time-consuming and not suitable for measuring dynamic scenes. The coded aperture snapshot spectral imager (CASSI) can capture spectral imaging of dynamic scenes by a single-frame exposure, which has a lot of attention due to its ability to recover the three-dimensional spatiospectral data cube from a snapshot two-dimensional coded aperture projection [5–8]. The reason is that the scene which is modulated by coded aperture and dispersive element is spatially and spectrally sparse and can be reconstructed by the CS (compressed sensing) theory [9–11]. At present, CASSI is mostly focused on the visible spectrum operating in 400–700 nm band. In comparison to visible spectrum, the short -wave infrared spectrum has a unique advantage in dealing

with the interference of aerosol, fog and smoke, which is conducive to long -distance detection. Limited by the compatible optical materials and detectors [12], the research of short-wave infrared CASSI is rarely reported. Considering the anti-interference advantage of the short-wave infrared CASSI, it is both important and urgent to research it.

Common to all spectral imaging system, the dispersive element design is one of the most important factors in the performance of CASSI system. The dispersive elements of CASSI are referred to plane grating or double Amici with a direct view [7, 13, 14]. But when these dispersive elements are used, optical systems of CASSI tend not to be compact due to the adding of collimating and imaging lens as shown in the dotted box in Fig. 1, especially for long focal length optical systems. Therefore, we intend to use the basic Offner imaging spectrometer which is a unit magnification system, providing a compact form and a small fraction of spectral and spatial distortions, to replace the collimating lens, the dispersion element and the imaging lens. However, LOBB has shown that the basic Offner imaging spectrometer works only in a thin annular region [15]. The optical system of CASSI based on the basic Offner spectrometer cannot present perfect imaging quality on account of the traditional entrance slit which is replaced by a square or rectangle coded aperture, so we need a wider annular region to ensure the perfect imaging quality. The annular region will be expanded if the system remains nearly telecentric in a wider region and this can be achieved by adding a concentric meniscus lens to the basic Offner imaging spectrometer, namely Offner–Wynne imaging spectrometer [16]. Finally, we applied it in a short-wave infrared CASSI to provide support for compact design and aberration reduction.

In this paper, we focus on the optical design of a short-wave infrared CASSI operating in 900–1700 nm band. It should be pointed out that the calculation model established by us can effectively obtain the optical parameters of meniscus lens, and an initial structure of the Offner–Wynne imaging spectrometer can be acquired. The Offner–Wynne imaging spectrometer can ensure perfect imaging quality in a wider annular region where the code aperture of the short-wave infrared CASSI can be placed perfectly. Then, a complete optical system of a short-wave infrared CASSI is designed through integrated optimization based on the the Offner–Wynne imaging spectrometer. In addition, the short-wave infrared band is invisible, so we must reduce the difficulty of adjustment. For this reason, we need more rigorous tolerance allocation and analysis to ensure the relatively loose tolerance requirements in optical design [17].

2. Principle

The optical system of representative CASSI is realized by an objective lens, a coded aperture, a collimating lens, a dispersive element, an imaging lens and a focal plane array detector. The principle layout of CASSI system is shown in Fig. 1. The 3D source information is imaged on the plane of the coded aperture by the objective lens, x and y index of the spatial coordinates and λ index of the wavelength coordinate. The coded aperture performs a spatial modulation over all wavelengths in the spectral cube of the source information [18]. The spatially modulated light is dispersed by the dispersive

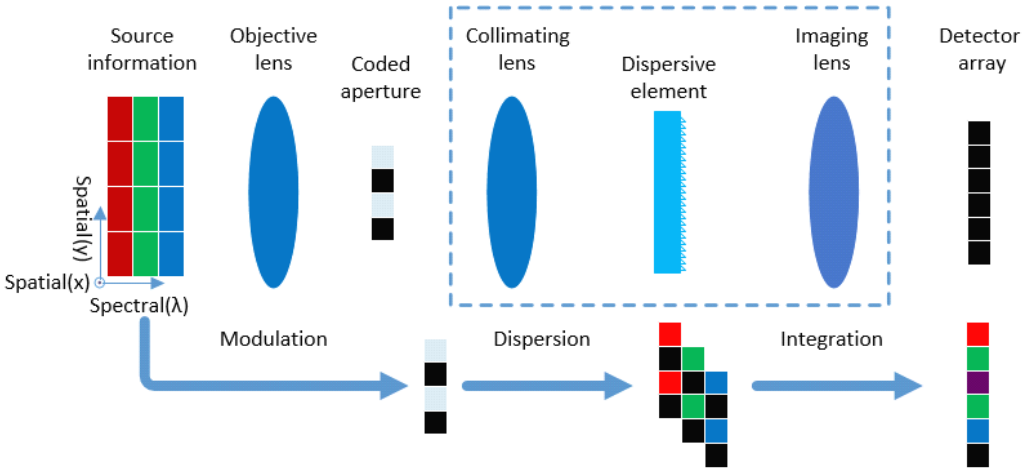

Fig. 1. Schematic diagram of CASSI.

element after propagation through the collimating lens. It is generally supposed that the dispersion is along one direction of the detector. Ultimately, the multiple 2D intensity images of the code-modulated scene, wavelength-dependent are integrated on the plane of the detector array by the imaging lens.

Generally, collimating lens and imaging lens contain multitude optical elements for collimating and converging light, which make the whole optical system of CASSI complex. Unlike previous design, in order to improve the transmittance and image quality of the optical system, we apply the Offner–Wynne imaging spectrometer to the short -wave infrared CASSI instead of the collimating lens, the dispersive element and the imaging lens. The Offner–Wynne imaging spectrometer can be achieved by adding a concentric meniscus lens to the basic Offner imaging spectrometer.

Compared to the basic Offner imaging spectrometer, the Offner–Wynne imaging spectrometer reduces the spectral smile across the entire working band by adding a concentric meniscus lens, and allows to enlarge the spectral dimension of the image or to increase the grating density [19]. Due to the addition of a meniscus lens, the spherical aberration and overall Petzval sum can be greatly decreased [20, 21].

Therefore, in this paper, we propose a calculation model to achieve optical parameters of the meniscus lens, which can obtain the initial structure of the Offner–Wynne imaging spectrometer.

The optical system of the short-wave infrared CASSI we designed consists two parts: the objective lens and the Offner–Wynne imaging spectrometer. It should be pointed out that the code aperture is located on the image surface of the objective lens, that is, the object surface of the Offner–Wynne imaging spectrometer. Firstly, we design these two parts independently on the premise of parameter matching. And then we adopt the method of integrated optimization to provide further enhancement of the imaging quality of the entire optical system on the basis of guaranteeing the performance of these two independent parts.

T a b l e 1. Specific design parameters of the short-wave infrared CASSI.

Parameters	Value
Wavelength range	900–1700 nm
Focal length	1200 mm
F-number	≤ 6
Spectral resolution	≤ 20 nm
Field angle	≥ 0.6°
Spectral smile	< half a pixel
Keystone	< half a pixel

The optical system is designed to detect and analyze the spectral information of the plume from a distant target. Furthermore, we can monitor the real-time operation status of the target engine according to the spectral information of the plume. Based on the application background analysis, the specific design parameters are shown in Table 1.

3. Optical design

3.1. Optical design of the objective lens

The objective lens is designed in the form of telecentricity in image space to ensure that the chief ray in each field can be vertically incident on the code aperture. The relevant optical system parameters of the objective lens are restricted by specific design parameters of the short-wave infrared CASSI. Moreover, taking into account that the reduction ratio of the Offner–Wynne imaging spectrometer is 1, we used a code aperture of 20 μm pixel size with 512 × 512 pixels, and the pixel size of the short-wave infrared focal plane detector we used is equivalent to the code aperture and has 640 × 512 pixels considering the number of spectral bands. Therefore, the half-field angle of the objective lens can be obtained as follows:

$$\omega = \arctan\left(\frac{L}{2f'}\right) \tag{1}$$

where L is the diagonal dimension of the code aperture, f' is the focal length of the objective lens. So the field angle of the objective lens is $2\omega = 0.69°$. The relevant specific design parameters of the objective optics are shown in Table 2.

T a b l e 2. Specific design parameters of the objective lens.

Parameters	Value
Wavelength range	900–1700 nm
Focal length	1200 mm
F-number	6
Field angle	0.69°

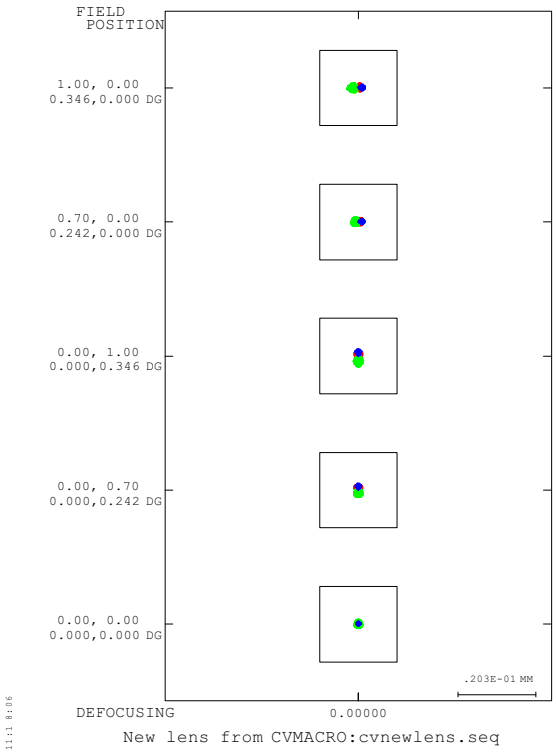

Fig. 2. Spot diagram of the objective lens.

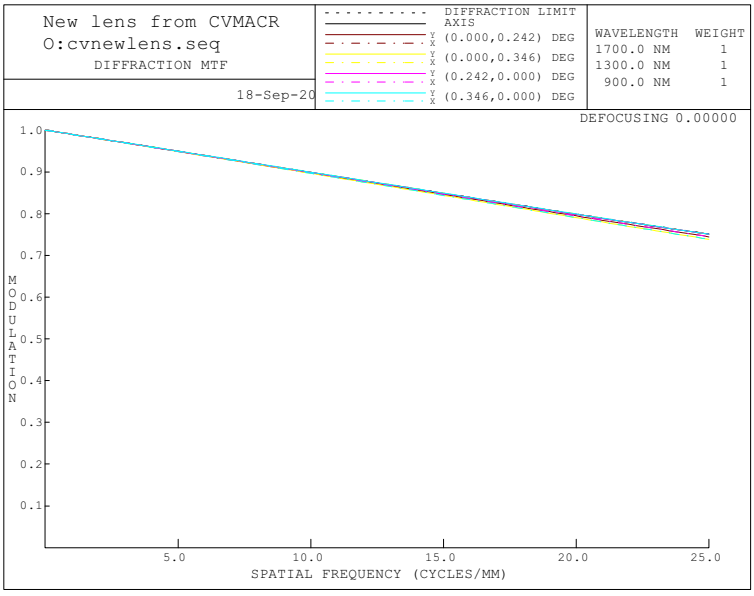

Fig. 3. MTF of the objective lens.

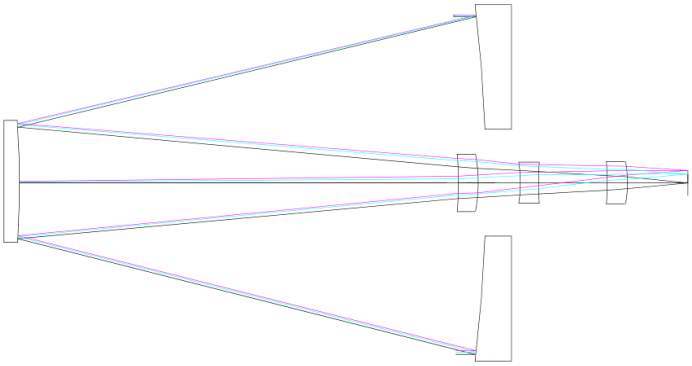

Fig. 4. Objective lens.

During the next optimization process, the telecentric path in image space, the focal length and the image size are used as constraint conditions, and the performance of the objective lens is evaluated by spot diagrams and the modulation transfer function (MTF). In Fig. 2, the spot diagram of the objective lens presents that the spots are well focused within a 20 μm pixel represented by the square in each field of view. The MTF curve of the objective lens is shown in Fig. 3, and the cutoff frequency is 25 lp/mm. The curve indicates that the MTF is higher than 0.75 in each field of view.

The final design result shown in Fig. 4, and the objective lens we designed, has an excellent performance and meets the specific design parameters based on the above analysis.

3.2. Optical design of the Offner–Wynne imaging spectrometer

The Offner–Wynne imaging spectrometer, as the spectroscopic lens of the short-wave infrared CASSI, determines the spectral resolution of the whole optical system. In order to obtain the initial structure of the Offner–Wynne imaging spectrometer, we propose a calculation model to achieve optical parameters of the meniscus lens based on the basic Offner imaging spectrometer.

Figure 5 shows that the basic Offner imaging spectrometer is composed of two spherical concentric elements: a concave mirror M used in double reflection and a convex diffraction grating G, and the concave mirror has twice the radius of the convex diffraction grating. The *YZ* plane represents the meridional section of the basic Offner imaging spectrometer.

The grating equation for arbitrary wavelength λ can be written as

$$\sin\beta + \sin\beta' = mg\lambda \tag{2}$$

where m is the diffraction order, g is the density of grating. The wavefront aberration of the basic Offner imaging spectrometer is formulated in terms of the optical path difference between the chief ray from the object O to the image I passing through arbitrary

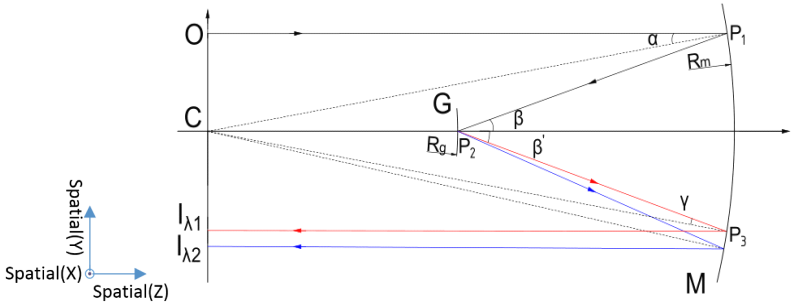

Fig. 5. The optical path of an arbitrary chief ray on a basic Offner imaging spectrometer.

points P_1, P_2, P_3 on the mirror M and grating G. By applying the Fermat principle, the wavefront aberration of the chief ray can be defined as [16, 22]

$$\sum F = F + F' + mg\lambda x = \overline{OP_1} + \overline{P_1P_2} + \overline{P_2P_3} + \overline{P_3I} + m\lambda N(x, y) \tag{3}$$

The wavefront aberration $\sum F$ is equivalent to the sum of the optical path difference and the phase retardation $m\lambda N(x, y)$ by the grating. The optical path difference comprised two terms: the optical path F before incidence on the grating and the optical path F' after diffraction. If the arbitrary object point $O(x, y)$ is arranged in the X axis which deduce the F to fourth-order in the spatial coordinates by considering an arbitrary meridional ray, F can be given by [23]

$$F(x, 0) = F(0, 0) - x\sin\beta + \frac{1}{8}\frac{\sin\beta}{R_g^3}(2\tan\alpha - \tan\beta)x^4 + O(x^5) \tag{4}$$

where R_g is the radius of grating G, and α, β are incidence angles in mirror M and grating G. The corresponding image point $I(x', y')$ is also arranged in the X axis, F' can be given by

$$F'(x, 0) = F'(0, 0) - x'\sin\beta' + \frac{1}{8}\frac{\sin\beta'}{R_g^3}(2\tan\gamma - \tan\beta')x'^4 + O(x'^5) \tag{5}$$

where β' is the angle of diffraction in grating G, γ is the incidence angle on the point P_3 which is in mirror M. Using Eq. (4) and Eq. (5), the complete fourth-order term is written as

$$\sum F_4 = \frac{1}{8}\frac{\sin\beta}{R_g^3}(2\tan\alpha - \tan\beta)x^4 + \frac{1}{8}\frac{\sin\beta'}{R_g^3}(2\tan\gamma - \tan\beta')x'^4 \tag{6}$$

Since the ray transverse aberration is proportional to the spatial derivatives of the aberration function and assuming that the RMS spot radius (R_{rms}) is a measure of ray aberration for rays crossing the pupil border, the R_{rms} is defined as [23]:

$$R_{\mathrm{rms}} = \frac{C}{(f^{\#})^3}\left[\sin\beta(2\tan\alpha - \tan\beta) + \sin\beta'(2\tan\gamma - \tan\beta')\right] \tag{7}$$

where C is a constant and it has been taken into account that the F-number ($f^{\#}$) is inversely proportional to the grating aperture diameter.

Figure 6 shows the Offner–Wynne imaging spectrometer which includes a concentric meniscus lens (ML), a concave mirror (M) and a convex diffraction grating (G) with their centres of curvature coincident. It is assumed that ML and M are used in both object and image spaces, G is deposited among them.

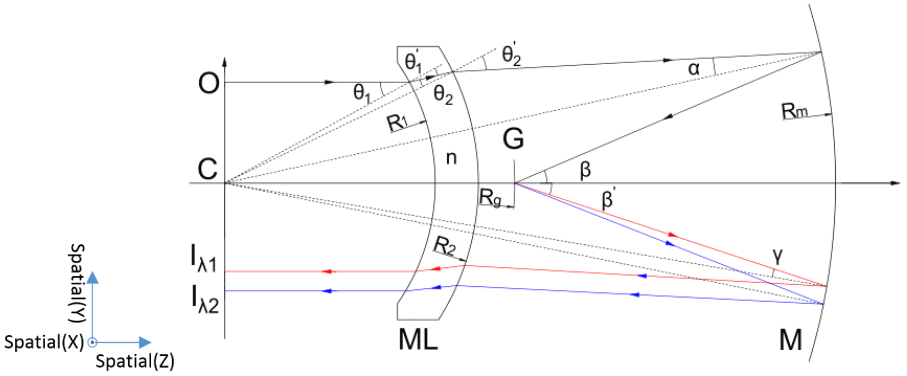

Fig. 6. The optical path of an arbitrary chief ray on an Offner–Wynne imaging spectrometer.

Similarly, a chief ray from object point $O(x, y)$ enters the optical system in parallel to the optical axis Z, passing through ML twice, M twice and G. In this case, the relationship between these angles can be determined by applying the law of sines and Snell's law. This allows us to write:

$$\sin\theta_1 = n\sin\theta_1' \tag{8a}$$

$$\sin\theta_2' = n\sin\theta_2 \tag{8b}$$

$$\sin\alpha = R_2\sin\theta_2'/R_{\mathrm{m}} \tag{9a}$$

$$\sin\theta_2 = R_1\sin\theta_1'/R_2 \tag{9b}$$

$$\sin\gamma = R_{\mathrm{g}}\sin\beta'/R_{\mathrm{m}} \tag{10a}$$

$$\sin\beta = R_{\mathrm{m}}\sin\alpha/R_{\mathrm{g}} \tag{10b}$$

Where n is the refraction index of ML and R_1, R_2, R_{m} and R_{g} are the radius of the lens inner surface, lens outer surface, concave mirror and convex diffraction grating, respectively. Incidence angles (θ_1, θ_2) correspond to refraction angles (θ_1', θ_2') in inner and

outer surfaces of ML. The incidence angle β corresponds to the diffraction angel β' in G. α, γ are incidence angles of M.

Combing Eqs. (2), (7), (8), (9) and (10), we can derive RMS spot radius (R_{rms}) of the chief ray as

$$R_{\mathrm{rms}} = \frac{C}{(f^{\#})^3}\left[\frac{2R_1^2\sin^2\theta_1}{R_{\mathrm{g}}\sqrt{R_{\mathrm{m}}^2 - R_1^2\sin^2\theta_1}} - \frac{R_1^2\sin^2\theta_1}{R_{\mathrm{g}}\sqrt{R_{\mathrm{g}}^2 - R_1^2\sin^2\theta_1}} + \frac{2ab}{\sqrt{1-b^2}} - \frac{a^2}{\sqrt{1-a^2}}\right] \tag{11}$$

where $a = \dfrac{R_{\mathrm{g}}g\lambda - R_1\sin\theta_1}{R_{\mathrm{g}}}$ and $b = \dfrac{R_{\mathrm{g}}g\lambda - R_1\sin\theta_1}{R_{\mathrm{m}}}$.

Equation (11) shows that the RMS spot radius (R_{rms}) of the Offner–Wynne imaging spectrometer depends on the parameters of R_1, R_{g}, R_{m}, θ_1, $f^{\#}$, g and λ. Wavelength λ, incidence angle θ_1, grating density g and F-number $f^{\#}$ are determined by the specific design parameters of the short-wave infrared CASSI. Radius R_{g} and R_{m} can be calculated by the equation $R_{\mathrm{m}}^2/4R_{\mathrm{g}}^2 + h_0^2/R_{\mathrm{m}}^2 = 1$ and $R_{\mathrm{m}}/R_{\mathrm{g}} < 2$ [24]. Therefore, R_{g}, R_{m}, θ_1, $f^{\#}$, g and λ can be obtained according to the above analysis, and then the radius R_1 of the meniscus lens can be calculated by Eq. (11).

In Fig. 7, $R_{\mathrm{g}} = 202$ mm, $R_{\mathrm{m}} = 400$ mm, $\lambda = 1300$ nm, $g = 50$ lp/mm, $\theta_1 = 30°$, and $f^{\#} = 6$, the radius R_1 is plotted as a function of RMS spot radius (R_{rms}) based on Eq. (11). It is clear from Fig. 7 that the RMS spot radius (R_{rms}) is much faster for large solutions when R_1 changes from its best value. Therefore, depending on the minimum value of RMS spot radius (R_{rms}), we can obtain the unique solution of radius $R_1 = 145$ mm as its optimal initial solution.

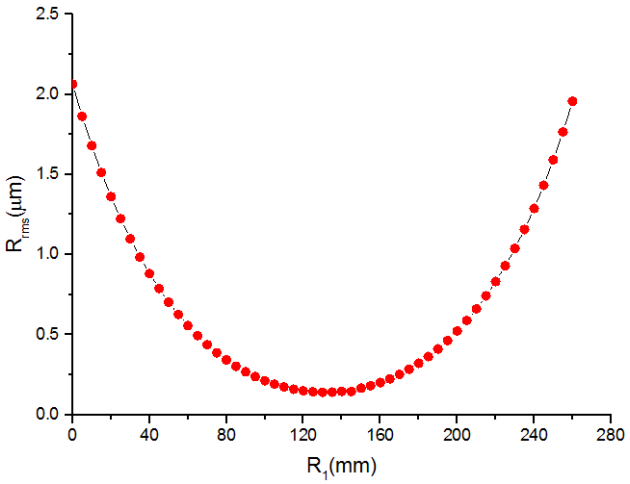

Fig. 7. RMS spot radius R_{rms} *versus* radius R_1 for the Offner–Wynne imaging spectrometer.

On the other hand, the focal power φ of a meniscus lens and its derivative $\mathrm{d}\varphi/\mathrm{d}n$ are:

$$\varphi = (n-1)\left(\frac{1}{R_1} - \frac{1}{R_2}\right) + \frac{d(n-1)^2}{2R_1R_2} \tag{12}$$

$$\frac{\mathrm{d}\varphi}{\mathrm{d}n} = \left(\frac{1}{R_1} - \frac{1}{R_2}\right) + \frac{d(n-1)^2}{n^2R_1R_2} \tag{13}$$

The chromatic aberration vanishes when the derivative equals 0. In this case, the following is obtained:

$$\frac{R_2 - R_1}{d} = \frac{n^2 - 1}{n^2} \tag{14}$$

In addition, the achromatic meniscus lens can be used to compensate the spherical aberration caused by the mirror in the condition of $n = 1.5$ [25], and the following is obtained:

$$R_2 - R_1 \approx 0.56d \tag{15}$$

Considering the weight, costs, manufacturing and adjustment, the diameter and center-thickness ratio of the meniscus lens is typically between 8:1 and 15:1. When the ratio approaches 15:1, costs begin to rise rapidly. Various factors considered, we selected the appropriate center-thickness $d = 20$ mm, and then $R_2 = 156.2$ mm could be acquired by Eq. (15).

Finally, parameters of meniscus lens, namely radius R_1, R_2 and center-thickness d, are determined based on the calculation model. It should be pointed out that many factors in the actual optical structure will affect the value of the thickness d, the radius R_1 and R_2, and the values obtained via theoretical calculations simply allowed determination of a good initial structure.

In the subsequent design process, we used this initial structure in combination with the constraint conditions: such as telecentric path in object space and image space, the reduction ratio and the object size, to take further optimization. The relevant specific design parameters of the Offner–Wynne imaging spectrometer are shown in Table 3.

T a b l e 3. Specific design parameters of the Offner–Wynne imaging spectrometer.

Parameters	Value
Wavelength range	900–1700 nm
Reduction ratio	1
F-number	6
Object height	10.2 mm
Average spectral resolution	16 nm
Grating groove density	50 lp/mm

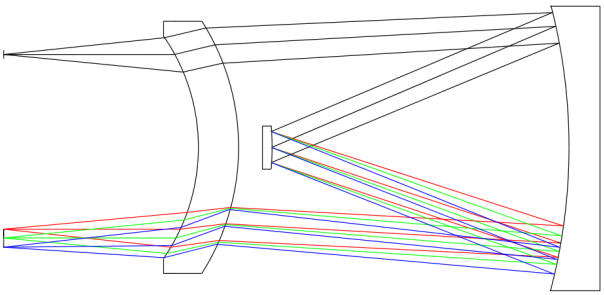

Fig. 8. The Offner–Wynne imaging spectrometer.

The final design result shown in Fig. 8, and the performance of the Offner–Wynne imaging spectrometer are evaluated by spot diagrams and the modulation transfer function (MTF). The spot diagram in each field of view is shown in Fig. 9 and squares represent each pixel of 20 μm. Figure 9 indicates that the spots are all well focused within a single pixel. Figure 10 shows the MTF curves for the wavelength 1300 nm, wavelength 1700 nm and wavelength 900 nm. The figure shows that the MTF is higher than 0.7 in each field of view at 25 lp/mm.

In addition, the values of the spectral smile and the spectral keystone are also an essential measurement index for spectral imaging system. This paper obtains the spectral

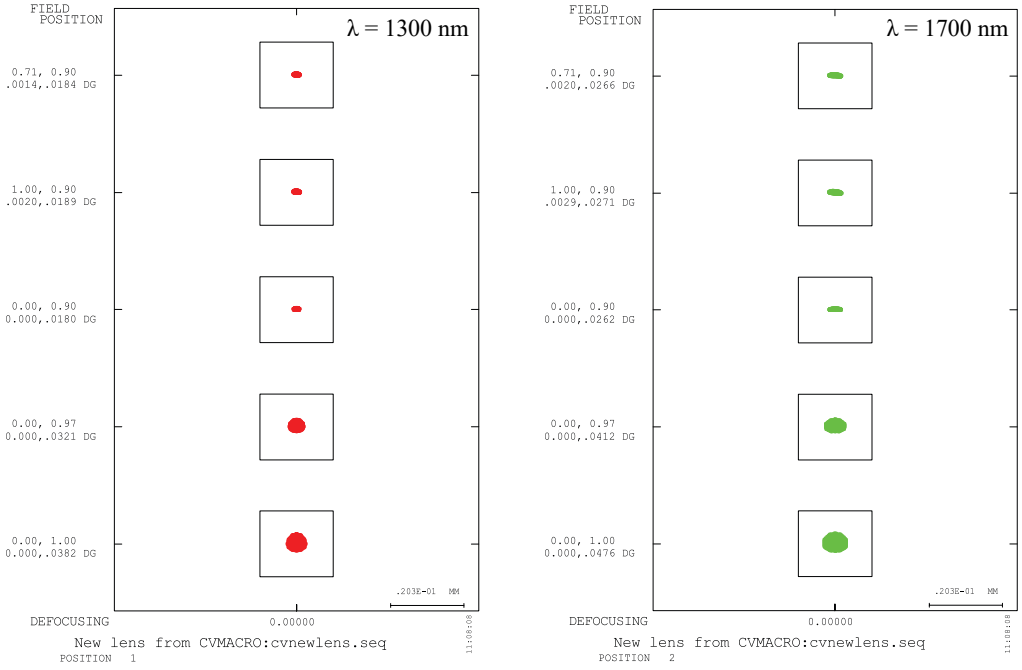

Fig. 9. Spot diagram of the Offner–Wynne imaging spectrometer.

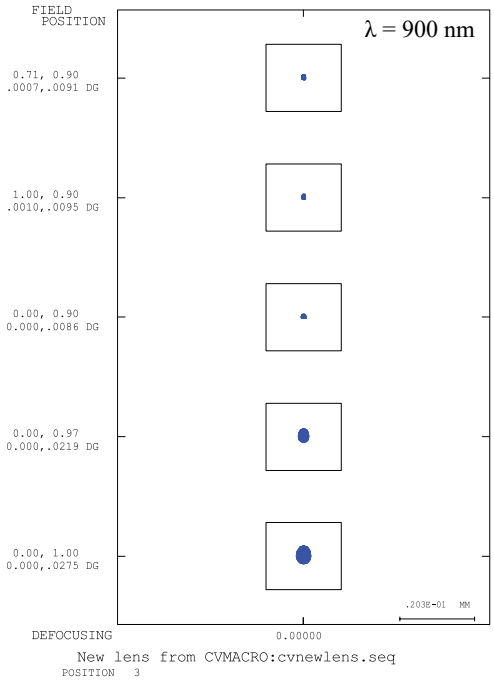

Fig. 9. Continued.

smile and spectral keystone values of the system via real ray tracing, as shown in Table 4. It indicates that the spectral smiles in the 900–1700 nm wavelength range are less than 6 μm, which are almost confined within a quarter of a pixel. The spectral key-

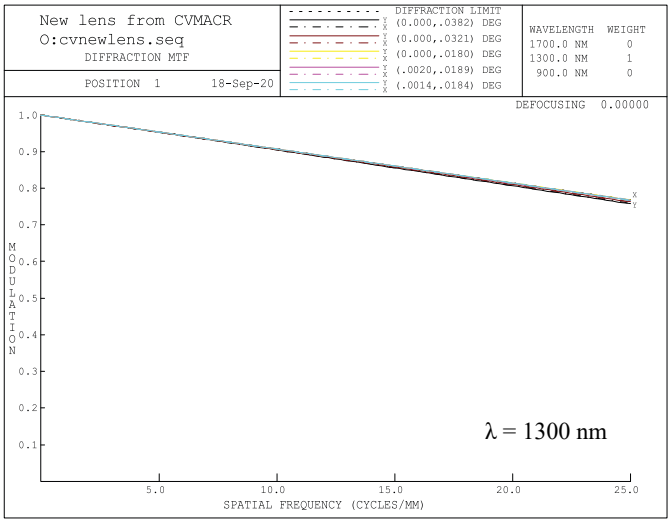

Fig. 10. MTF of the Offner–Wynne imaging spectrometer.

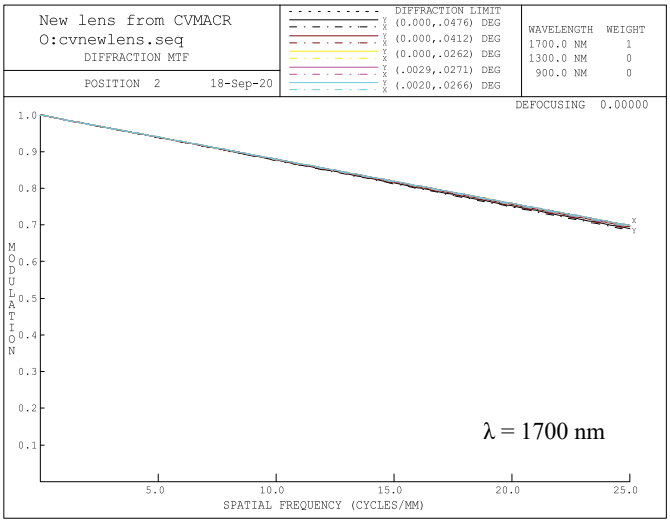

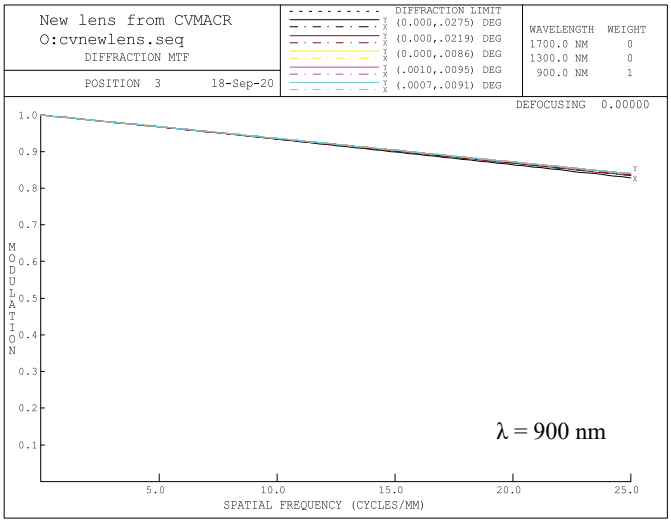

Fig. 10. Continued.

T a b l e 4. Spectral smile (μm) of the Offner–Wynne imaging spectrometer with wavelength λ and normalized field ω.

λ [nm]	900	1000	1100	1200	1300	1400	1500	1600	1700
$\omega = 0.7$	3.2	2.9	2.8	2.7	2.5	2.3	2.1	1.9	1.8
$\omega = 1$	5.6	5.2	4.8	4.7	4.5	4.2	3.9	3.8	3.5

stone of the system is less than 8 μm throughout the entire wavelength band. Hence, the spectral smile and the spectral keystone are less than half a pixel, signifying there is no need for data processing correction.

3.3. Integrated optimization of optical system

The objective lens and the Offner–Wynne imaging spectrometer have the same *F*-number, and their pupil matches well owing to the design of telecentricity, so the two systems can be combined perfectly. However, on account that the objective lens and the Offner–Wynne imaging spectrometer have different characteristics, it is necessary to balance the combinational aberrations based on the following process which is called integrated optimization. Code-V was used to adjust the system parameters and ensure that the sizes of these aberrations after combination remain within the allowable range. The results of optical design after integrated optimization are shown in the following Fig. 11. The aperture stop is located on the first surface of the optical system.

The system's MTFs of 1300, 1700 and 900 nm are charted in Fig. 12, and the MTFs are all greater than 0.65 at the Nyquist frequency of 25 lp/mm.

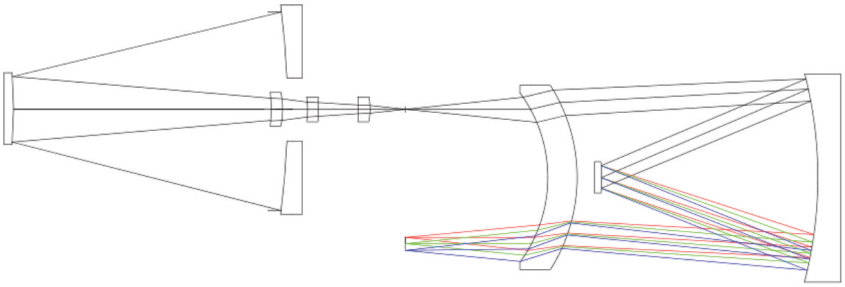

Fig. 11. Optical system of the short-wave infrared CASSI.

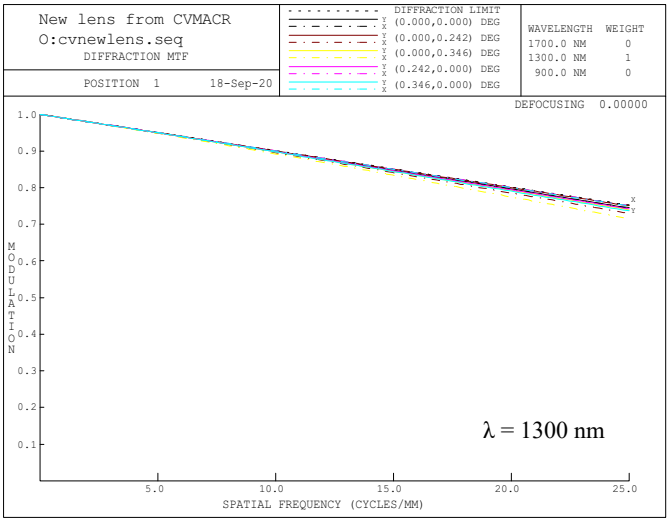

Fig. 12. MTFs of final design with wavelength.

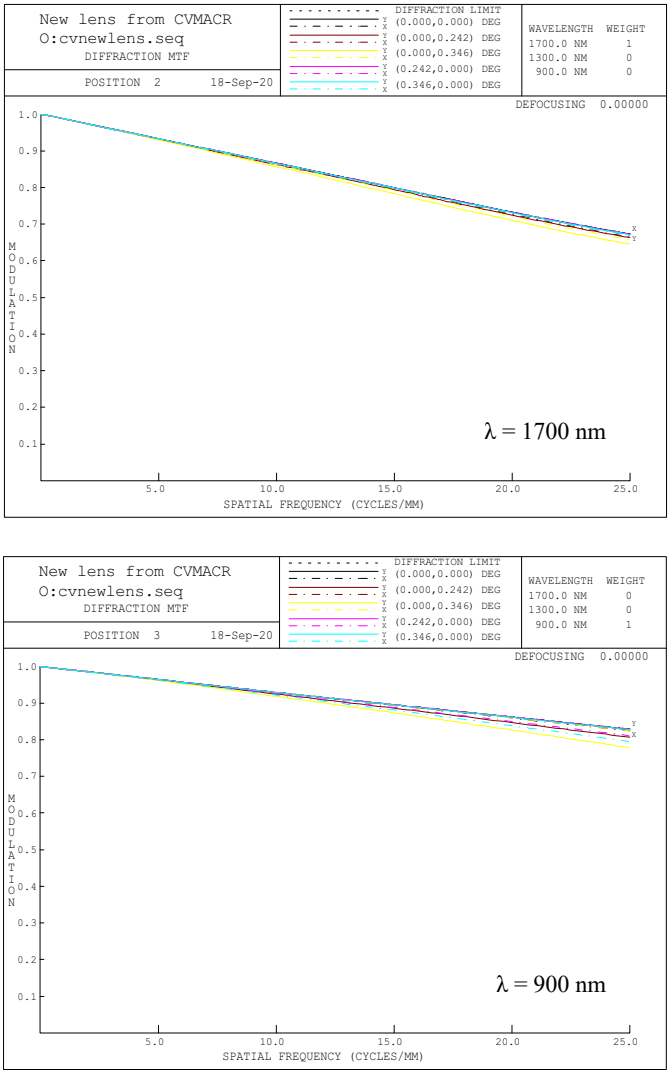

Fig. 12. Continued.

The spot diagrams indicate how dispersed light images on the focal plane and the spots at each wavelength are given in Fig. 13. Squares represent each pixel of 20 μm at each wavelength and the spots in each field of view are all focused within one pixel.

Finally, we used the MTF tolerance analysis for the central wavelength of 1300 nm to analyze the tolerance sensitivity of the optical system as shown in Fig. 14. It is generally recognized that the tolerance analysis indicates the feasibility of practical application of optical systems. The results show that the MTF of the optical system has

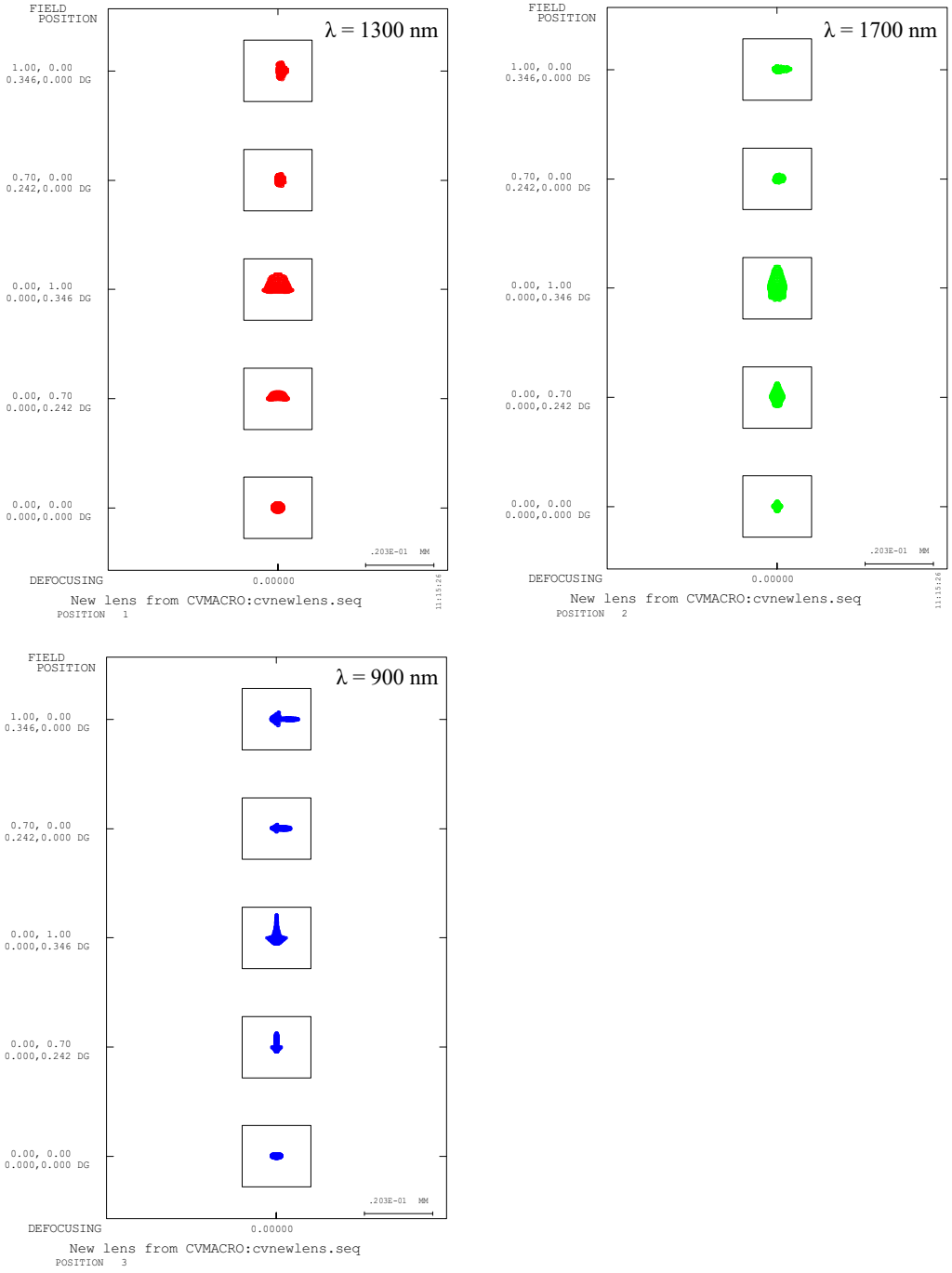

Fig. 13. The spot diagrams of final design with wavelength.

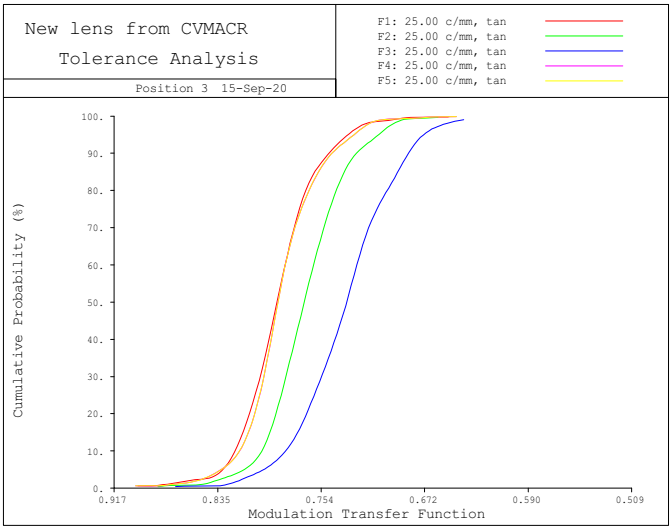

Fig. 14. MTF tolerance analysis of final design with central wavelength.

a probability of 99% above a value of 0.62 under the default tolerance allocation conditions. In other words, the optical system meets the requirements for practical application.

4. Conclusion

In this paper, an improved optical system of the short-wave infrared CASSI is designed which includes the objective lens and the Offner–Wynne imaging spectrometer with a meniscus lens. In addition, a calculation model which provides a simple approach to achieve the optical parameters of meniscus lens is proposed based on calculating the RMS spot radius (R_{rms}) of the Offner–Wynne imaging spectrometer. The calculation model has a great flexibility of work and designs for different parameters as the F-number, the wavelength, the incidence angle, the grating density and the radius, which shows its versatility, and can obtain an excellent initial structure of the Offner–Wynne imaging spectrometer. In the subsequent design process, we adopted an independent design firstly, and then adopted an integration optimization method to design the optical system of the short-wave infrared CASSI. The spot sizes at each field are far less than 20 μm, ensuring that the energy is all concentrated in one pixel, the MTFs at each wavelength are all greater than 0.68, and the spectral smile of the system is less than 6 μm. In short, the presented design results illustrate that the performance of the short-wave infrared CASSI is excellent and meets the practical application requirements.

Funding
National Natural Science Foundation of China (61805275).

Conflicts of interest/Competing interests
On behalf of all authors, the corresponding author states that there is no conflict of interest.

Code availability
The data and material used during the current study are available from the corresponding author on reasonable request.

Authors' contribution
Chong Song (songchong124@163.com) contributed to the conception of the study and completed the optical design; Liang Zhou (zhouliang@opt.ac.cn) completed the derivation of relevant formulas; Zhaohui Liu (lzh@opt.ac.cn) contributed significantly to analysis and manuscript preparation; Kai Jiang (jiangkai2008.jj@163.com) performed the data analyses and wrote the manuscript; Kai Liu (sglika@163.com) provided constructive discussions and revised the manuscript.

References

[1] WU T., LI G., YANG Z., ZHANG H., LEI Y., WANG N., ZHANG L., *Shortwave infrared imaging spectroscopy for analysis of ancient paintings*, Applied Spectroscopy **71**(5), 2017, pp. 977–987.
[2] CUI J., TANG Y., HAN P., PAN M., ZHANG J., *Development of diagnostic imaging spectrometer for tumor on-line operation*, Optics and Precision Engineering **21**(12), 2013, pp. 3043–3049 (in Chinese).
[3] PLAZA A., BENEDIKTSSON J.A., BOARDMAN J.W., BRAZILE J., BRUZZONE L., CAMPS-VALLS G., CHANUSSOT J., FAUVEL M., GAMBA P., GUALTIERI A., MARCONCINI M., TILTON J.C., TRIANNI G., *Recent advances in techniques for hyperspectral image processing*, Remote Sensing of Environment **113**, 2009, pp. S110–S122, DOI: 10.1016/j.rse.2007.07.028.
[4] GOWEN A.A., O'DONNELL C.P., CULLEN P.J., DOWNEY G., FRIAS J.M., *Hyperspectral imaging–an emerging process analytical tool for food quality and safety control*, Trends in Food Science & Technology **18**(12), 2007, pp. 590–598, DOI: 10.1016/j.tifs.2007.06.001.
[5] EICHENHOLZ J.M., BARNETT N., JUANG Y., FISH D., SPANO S., LINDSLEY E., FARKAS D.L., *Real-time megapixel multispectral bioimaging*, Proceedings of SPIE **7568**, 2010, article 75681L, DOI: 10.1117/12.842563.
[6] GAO L., KESTER R.T., HAGEN N., TKACZYK T.S., *Snapshot image mapping spectrometer (IMS) with high sampling density for hyperspectral microscopy*, Optics Express **18**(14), 2010, pp. 14330–14344, DOI: 10.1364/OE.18.014330.
[7] WAGADARIKAR A., JOHN R., WILLETT R., BRADY D., *Single disperser design for coded aperture snapshot spectral imaging*, Applied Optics **47**(10), 2008, pp. B44–B51, DOI: 10.1364/AO.47.000B44.
[8] KITTLE D., CHOI K., WAGADARIKAR A., BRADY D.J., *Multiframe image estimation for coded aperture snapshot spectral imagers*, Applied Optics **49**(36), 2010, pp. 6824–6833, DOI: 10.1364/AO.49.006824.
[9] CANDÈS E.J., *Compressive sampling*, [In] *Proceedings of the International Congress of Mathematicians*, 2006, pp. 1433–1452.
[10] LIN X., WETZSTEIN G., LIU Y., DAI Q., *Dual-coded compressive hyperspectral imaging*, Optics Letters **39**(7), 2014, pp. 2044–2047, DOI: 10.1364/OL.39.002044.
[11] WAGADARIKAR A.A., PITSIANIS N.P., SUN X., BRADY D.J., *Video rate spectral imaging using a coded aperture snapshot spectral imager*, Optics Express **17**(8), 2009, pp. 6368–6388, DOI: 10.1364/OE.17.006368.
[12] SUN X., ABSHIRE J.B., BECK J.D., MITRA P., REIFF K., YANG G., *HgCdTe avalanche photodiode detectors for airborne and spaceborne lidar at infrared wavelengths*, Optics Express **25**(14), 2017, pp. 16589–16602, DOI: 10.1364/OE.25.016589.

[13] Rueda H., Arguello H., Arce G., *DMD-based implementation of patterned optical filter arrays for compressive spectral imaging*, Journal of the Optical Society of America A **32**(1), 2015, pp. 80–89, DOI: 10.1364/JOSAA.32.000080.
[14] Kittle D.S, Marks D.L, Brady D.J., *Design and fabrication of an ultraviolet-visible coded aperture snapshot spectral imager*, Optical Engineering **51**(7), 2012, article 071403, DOI: 10.1117/1.OE.51.7.071403.
[15] Lobb D.R., *Theory of concentric designs for grating spectrometers*, Applied Optics **33**(13), 1994, pp. 2648–2658, DOI: 10.1364/AO.33.002648.
[16] Prieto-Blanco X., de la Fuente R., *Compact Offner–Wynne imaging spectrometers*, Optics Communications **328**, 2014, pp. 143–150, DOI: 10.1016/j.optcom.2014.04.060.
[17] Jianjun Chen, Jin Yang, Jianan Liu, Jianli Liu, Ci Sun, Xiaotian Li, Bayanheshig, Jicheng Cui, *Optical design of a short-wave infrared prism-grating imaging spectrometer*, Applied Optics **57**(34), 2018, pp. F8–F14, DOI: 10.1364/AO.57.0000F8.
[18] Arce G.R., Brady D.J., Carin L., Arguello H., Kittle D.S., *Compressive coded aperture spectral imaging: an introduction*, IEEE Signal Processing Magazine **31**(1), 2014, pp. 105–115, DOI: 10.1109/MSP.2013.2278763.
[19] Lucke R.L., *Out-of-plane dispersion in an Offner spectrometer*, Optical Engineering **46**(7), 2007, article 073004, DOI: 10.1117/1.2754316.
[20] Prieto-Blanco X., Montero-Orille C., Couce B., de la Fuente R., *Analytical design of an Offner imaging spectrometer*, Optics Express **14**(20), 2006, pp. 9156–9168, DOI: 10.1364/OE.14.009156.
[21] Ku H., Kim S.H., Kong H.J., Lee J.H., *Optical design, performance, tolerancing of an Offner imaging spectrograph*, Proceedings of SPIE **8491**, 2012, article 84910K, DOI: 10.1117/12.929483.
[22] Lobb D.R., *Imaging spectrometers using concentric optics*, Proceedings of SPIE **3118**, 1997, pp. 339–347, DOI: 10.1117/12.283838.
[23] González-Núñez H., Prieto-Blanco X., de la Fuente R., *Pupil aberrations in Offner configurations*, Journal of the Optical Society of America A **29**(4), 2012, pp. 442–449, DOI: 10.1364/JOSAA.29.000442.
[24] Chrisp M.P., *Convex diffraction grating imaging spectrometer*, U.S. Patent, 5,880,834, 9 (1999).
[25] Zhou Y., *Applied Optics*, Publishing House of Electronics Industry, Beijing, 2011.

Received October 10, 2020